Self-consistent, analytic, periodic-loop-antenna theory

Satish Puri

IPP 4/214 November 1983

MAX-PLANCK-INSTITUT FÜR PLASMAPHYSIK

8046 GARCHING BEI MÜNCHEN

MAX-PLANCK-INSTITUT FÜR PLASMAPHYSIK

GARCHING BEI MÜNCHEN

Self-consistent, analytic, periodic-loop-antenna theory

Satish Puri

IPP 4/214 November 1983

Die nachstehende Arbeit wurde im Rahmen des Vertrages zwischen dem Max-Planck-Institut für Plasmaphysik und der Europäischen Atomgemeinschaft über die Zusammenarbeit auf dem Gebiete der Plasmaphysik durchgeführt.

IPP 4/214 Satish Puri

Self-consistent, analytic, periodic-loop-antenna theory

November 1983

Loop antenna coupling to toroidal plasmas is simulated in a flat geometry by an infinitely repeated array of finite loops in order to obtain a discrete spectrum along the y (azimuthal) as well as the z (toroidal) directions. The electromagnetic field of the entire configuration, including the wall, the plasma, and the Faraday shield, is analytically expressed in terms of the antenna current. The self-consistent antenna current is determined via variational techniques which also yield the antenna impedance. Finally, the theory is specifically applied to the case of ion-cyclotron-wave coupling.

1. INTRODUCTION

Recent contributions[1-13] to the loop-antenna theory have led to the following important realizations:

i) A two-dimensional sheet current model is an inadequate description of a practically realizable antenna which of necessity must possess feeder elements. The field contribution from these feeders can not be ignored and it becomes imperative to resort to a three-dimensional analysis as pointed out by Bhatnagar et al.[12].

ii) An acceptable solution must incorporate a self-consistent determination of the antenna current. This requirement becomes critical near the resonances. An elegant approach for achieving this end using Storer's variational technique[14, 15] is described by Theilhaber and Jacquinot[13].

The present paper offers the following significant advances over the existing results:

i) The electromagnetic field is analytically determined. This serves to illustrate the precise importance of feeder currents as well as the need for the accurate knowledge of the antenna current distribution.

ii) A more realistic antenna spectrum is simulated by the periodic antenna. The principal difference is that the spectrum is not concentrated at $n_y=n_z=0$ as in the case of a single loop, but is distributed over discrete n_y, n_z values, where n_y and n_z are the components of the refractive index $\underline{n}$ in the y and z directions, respectively.

iii) Considerable computational advantage may result from this discretization because the integrations in the y and z directions are now reduced to summations. The plasma surface impedance for the (n_y,n_z) refractive indices pairs can now be computed and stored and subsequently recalled instead of requiring a fresh determination during each iteration.

In other particulars this treatment resembles that of Ref. 13. Specifically, the variational principle developed by Storer[14, 15] is used for the determination of the antenna input impedance. However, we use a more general expression for the antenna current with complex amplitudes to allow for spatial phase differences among the harmonics.

Unless otherwise stated, the MKS system of units is employed. However, in order to avoid unnecessary clutter, all lengths have been normalized by multiplying through with $k_o=2\pi/\lambda_o$, where λ_o is the free-space wavelength. Also the angular frequency ω and the free-space impedance are

set to unity. The exponential variation $\exp\left[i(n_y y + n_z z - \omega t)\right]$ and explicit functional dependence on the refractive index $\underline{n}$ or its components (n_x, n_y, n_z) are generally suppressed if unambiguous from the context. Impedance values conform to circuit theory usage and are obtained through conjugation of the results obtained by the $\exp(-i\omega t)$ ansatz. Unless explicitly stated, the summations extend over all integers from $-\infty$ to ∞.

For the sake of notational simplification, the present analysis assumes that the antenna launches an evanescent spectrum of vacuum waves, i.e., n_{zo}, the fundamental refractive index along the z-direction exceeds unity. It is, however, a straightforward exercise to incorporate propagating waves within this description.

After outlining the geometry of the system in Sec. II, the electromagnetic field due to the loop antenna is derived in Sec. III. The full boundary value solution including the plasma, Faraday shield and wall effects is treated in Sec. IV. In Sec. V coupling to ICRF (ion cyclotron range of frequencies) waves is studied followed by a discussion of the results in Sec. VI.

II. THE IDEALIZED ANTENNA MODEL

Figure 1 shows the idealized, periodic loop antenna geometry. Each loop consists of an infinitesimally thin rectangular ribbon of height 2ℓ, breadth 2b and width 2w and possessing a resistivity R_A per unit length. It is driven by a "slice generator"[13-15] of voltage V situated at x=0, y=$-\ell$ and $-w \leq z \leq w$. The antenna is imaged indefinitely with periodicities Λ_{yo} and Λ_{zo} along the y- and z-directions, respectively.

The plasma is replaced by a smooth semi-infinite slab boundary at x=a with the surface impedance matrix

$$\underset{=P}{\zeta} = \begin{bmatrix} \zeta_{ff} & \zeta_{fs} \\ \zeta_{sf} & \zeta_{ss} \end{bmatrix} \qquad (1)$$

The significance of the matrix elements is discussed in Appendix A.

Faraday shielding is obtained by interposing a metallic screen (x=f) between the antenna and the plasma which selectively conducts along the z-direction and is perfectly insulating along the y-direction. Finally, the system is bounded by a wall at x=-c. The wall and the Faraday shield are assumed to possess surface impedances ζ_W and ζ_F, respectively. In addition to these idealizations, we will assume the absence of the transverse antenna current J_z^A.

III. ISOLATED ANTENNA IN FREE SPACE

It is convenient to introduce the unfolded antenna co-ordinate $-2(1+b) \leq \xi \leq 2(1+b)$ with origin at x=0, y=ℓ, as shown in Fig. 1a. The antenna current distribution $I(\xi)$ may be expressed as

$$I(\xi) = I_o f_\xi(\xi) f_z(z) , \tag{2}$$

where

$$f_\xi(\xi) = \sum_p F_\xi(p) \exp(i p n_{\xi o} \xi) , \tag{3}$$

$$f_z(z) = \sum_n F_z(n) \exp(i n n_{zo} z) , \tag{4}$$

$$n_{\xi o} = 2\pi / \Lambda_{\xi o} , \tag{5}$$

and

$$\Lambda_{\xi o} = 4(\ell + b) \tag{6}$$

Also by Fourier transformation one obtains

$$F_\xi(p) = \frac{1}{\Lambda_{\xi o}} \int_{-\Lambda_{\xi o}/2}^{\Lambda_{\xi o}/2} f_\xi(\xi) \exp(-i n_\xi \xi)\, d\xi , \qquad (7)$$

and,

$$F_z(n) = \frac{1}{\Lambda_{zo}} \int_{-\Lambda_{zo}/2}^{\Lambda_{zo}/2} f_z(z) \exp(-i n_z z)\, dz , \qquad (8)$$

where, $n_\xi = p\, n_{\xi o}$ and $n_z = n\, n_{zo}$. In order to allow for asymmetries in the current distribution, both $F_\xi(p)$ and $F_z(n)$ are, in general, complex. Note that this particular choice of $f_\xi(\xi)$ insures the continuity of antenna current including at $\xi = \pm 2(1+b)$ and no additional continuity constraints need be invoked.

The solution for the antenna electromagnetic field may now be obtained from the Maxwell's equations in vacuum, subject to the boundary condition that the magnetic field component H_z has a discontinuous jump at the location of the antenna current.

The total antenna field component Θ_ν^A, where

$$\underline{\underline{\Theta}}^A = \left[E_x^A \quad E_y^A \quad E_z^A \quad H_x^A \quad H_y^A \quad H_z^A \right], \qquad (9)$$

may be expressed in the form

$$\Theta_\nu^A = \Theta_\nu^{AF} + \Theta_\nu^{AB} + \left[\Theta_\nu^{AS}{}_b + \Theta_\nu^{AS}{}_{-b} + \Theta_\nu^{AS}{}_o + \Theta_\nu^{AS}{}_T\right], \quad (10)$$

where θ^{AF}, θ^{AB} and θ^{AS} pertain to the contributions from the antenna front surface, the antenna back and the two antenna sides taken together, respectively. We will see later that the field arising from the antenna sides has four distinct components; corresponding to a transmission line field $\theta^{AS}{}_T$ plus the contributions $\theta^{AS}{}_b$ and $\theta^{AS}{}_{-b}$ from the open circuit terminations at x=b and x=-b, respectively, and finally the contribution $\theta^{AS}{}_o$ due to the discontinuity at the input drive. In the following sections, we enlarge upon the description of each of these contributions.

A. Contributions from antenna front and back

From (2)-(4) one obtains the spectral distribution of current at $x=\pm b$ as

$$J_{\pm b}^A = \mp \frac{n_{yo}}{\pi} \sum_m \sum_n \sum_p \frac{F(n)F(p)}{n_y \pm n_3} \sin\left[(n_y \pm n_3)\ell\right] \cdot \exp\left[\pm i n_3 (\ell+b)\right] \exp\left[i(n_x x + n_y y + n_z z)\right] \quad (11)$$

where $n_y = mn_{yo}$ and $n_{yo} = 2\pi/\Lambda_{yo}$. Successive application of the boundary conditions for the tangential components of θ^A at $x = \pm b$ determines the electromagnetic fields due to the currents in the antenna front and back.

B. Contributions from the antenna sides

In the upper antenna arms, $\xi = x$ so that the current

$$I(\xi) = \bar{I}(x) \quad , \quad \text{for} \quad -b \leq \xi \leq b. \tag{12}$$

One may express I(x) as the superposition integral

$$I(x) = \int_{-\infty}^{\infty} \bar{I}(x - x')\, \delta(x')\, dx' \quad , \tag{13}$$

where $\delta(x)$ is the Dirac delta-function defined by the Fourier decomposition

$$\delta(x) = \frac{1}{2\pi} \int_{-\infty}^{\infty} \exp(i n_x x)\, dn_x \quad , \tag{14}$$

consisting of "elementary excitations" $\exp(in_x x)$. Observe that in the periodic loop antenna model, I(x), and hence the elementary excitations constitute endlessly repeated current sheets at intervals Λ_{yo} in the y-direction.

The procedure for obtaining θ^S involves the following steps:

i) Determining the electromagnetic field by solving Maxwell's equations subject to the boundary conditions at the current sheets due to an elementary excitation (Appendix B).

ii) Obtaining the Green's function, $G\theta\{\delta(x)\}$, i.e., the net response to the delta function excitation (14), by integrating the fields of the elementary excitations over $-\infty \leq n_x \leq \infty$ (Appendix B).

iii) Using the superposition integral

$$\int_{-\infty}^{\infty} I(x-x')\, G\theta\{\delta(x')\}\, dx' \qquad (15)$$

gives the electromagnetic field resulting from the current in (12).

iv) Finally, adding to (15) the field produced by the lower antenna arms yields the desired field θ^S. These last two steps involve a fair amount of algebra but no problem of principle; hence, their detailed derivation is omitted.

C. The total antenna field

Upon summing the field contributions Θ^{AF}, Θ^{AB} and Θ^{AS}, one obtains the composite antenna field. As explained already in (10), Θ^{AS} may be further split into four distinct components. For the E_y component of the antenna field, the various contributions are given as (see Appendix C for the remaining field components)

$$E_y^{AF} = i\,(n_{y_0}/2\pi) \sum_m \sum_n \sum_p F(n)\,F(p)\,\varepsilon(x-b) \cdot (n_y^2-1)\,N_x^{-1}\,(n_y+n_z)^{-1} \exp\{i n_z(\ell+b)\} \sin\{(n_y+n_z)\ell\}\,, \tag{16}$$

$$E_y^{AB} = -i\,(n_{y_0}/2\pi) \sum_m \sum_n \sum_p F(n)\,F(p)\,\varepsilon(x+b) \cdot (n_y^2-1)\,N_x^{-1}\,(n_y-n_z)^{-1} \exp\{-i n_z(\ell+b)\} \sin\{(n_y-n_z)\ell\}\,; \tag{17}$$

$$E_y^{AS_b} = -i\,(n_{y_0}/2\pi) \sum_m \sum_n \sum_p F(n)\,F(p)\,\varepsilon(x-b) \cdot N_x\,n_y\,(N_x^2+n_z^2)^{-1} \exp\{i n_z(\ell+b)\} \cdot \left[\sin\{(n_y+n_z)\ell\} + u_{x-b}\,(n_z/N_x)\cos\{(n_y+n_z)\ell\}\right]\,, \tag{18}$$

$$E_y^{AS_{-b}} = i\,(n_{y_o}/2\pi) \sum_m \sum_n \sum_p F(n)\,F(p)\,\xi(x+b)$$

$$\cdot N_x\, n_y\, (N_x^2 + n_\xi^2)^{-1} \exp\{-i n_\xi (\ell+b)\}$$

$$\cdot \left[\sin\{(n_y - n_\xi)\ell\} + u_{x+b}\,(n_\xi / N_x)\cos\{(n_y - n_\xi)\ell\}\right], \tag{19}$$

$$E_y^{AS_o} = i\,(n_{y_o}/2\pi) \sum_m \sum_n \sum_p F(n)\,F(p)\,\xi(x)$$

$$\cdot u_x\, n_y \left[\quad (\nu_x - i n_\xi)\right]^{-1} \exp(i n_y \ell)\sin\{2 n_\xi (\ell+b)\}, \tag{20}$$

and

$$E_y^{AS_\pi} = -i\,(n_{y_o}/2\pi) \sum_m \sum_n \sum_p F(n)\,F(p) \quad \left[n_\xi\{x - u_x(\ell+b)\} - n_y \ell\right]$$

$$\cdot 2\,\square(-b, b)\, n_y\, n_\xi\, (N_x^2 + n_\xi^2)^{-1} \exp\{i n_\xi u_x (\ell+b)\}, \tag{21}$$

where

$$N_x = |n_x|, \tag{22}$$

the "switch function"

$$u_x = \pm 1, \text{ for } x \gtrless 0, \tag{23}$$

$$\nu_x = u_x N_x \tag{24}$$

and the "box function"

$$\square(x_1 - x_2) = h(x_1) - h(x_2) \tag{25}$$

h(x) being the Heavyside "step function" defined as

$$\begin{aligned} h(x) &= 0 \quad , \quad \text{for} \quad x < 0 \, , \\ &= 1 \quad , \quad \text{for} \quad x \geq 0 \, , \end{aligned} \tag{26}$$

and

$$\xi(x) = \exp(-N_x |x|) \tag{27}$$

In (16)-(21) the common exponential dependence $\exp[i(n_y y + n_z z)]$ has been suppressed.

Following are some significant observations regarding the structure of the antenna field:

i) The field component pairs $(\theta^{AF}, \theta^{ASb})$ and $(\theta^{AB}, \theta^{AS-b})$ tend to cancel[16], leaving a net contribution which is of order $|\underline{n}|^{-2}$ compared to the individual contributions; thus confirming the importance of including the feeder currents in the analysis[1]. Ignoring feeder currents and using a current sheet antenna model instead would result in significantly

higher ($O|\underline{n}|^2$) fields for the given antenna current with seemingly superior coupling of radio-frequency energy into the plasma.

ii) The electric field component E_z is inherently present for $n_y \neq 0$. This effect is similar in origin to the case of E_z component of the electric field associated with a plane wave for finite n_y. Note that (see Appendix C) E_z vanishes identically for the case $n_\xi=0$, i.e., if one assumes the current to be constant over the antenna loop. But a closer look at the E_z^A expressions reveals that the presence of n_{yo} term accentuates the field at lower frequencies and one must forego the temptation of ignoring the finite wavelength effects even at low frequencies.

iii) Because of the delicate cancellation effects, an accurate determination of the self-consistent antenna current is apparently necessary[13]. An arbitrariness in the choice of the current profile may lead to substantial error in the field quantities.

D. The self-consistent current

We briefly outline Storer's[14, 15] variational principle used for the determination of the antenna current and the input impedance Z_A. The electric field along the antenna loop is given by

$$E_\xi(\xi) = R_A I(\xi) - V \delta(\xi - \xi_v) , \qquad (28)$$

where R_A is the antenna resistance per unit length, and V is the driving voltage located at ξ_v. Multiplying (28) by $I(\xi)$ and integrating around the loop gives the variational formulation

$$\oint E_\xi(\xi)\, I(\xi)\, d\xi = R_A \oint I^2(\xi)\, d\xi - V I(\xi_v) . \qquad (29)$$

Since $V = Z_A I(\xi_v)$, one finally obtains from (29)

$$Z_A I^2(\xi_v) + \oint E_\xi(\xi)\, I(\xi)\, d\xi - R_A \oint I^2(\xi)\, d\xi = 0 . \qquad (30)$$

Differentiating (30) with respect to the $F_\xi(p_i)$ term in the Fourier expansion (3), one obtains

$$2 Z_A \exp\left\{2i n_{\xi i}(\ell+b)\right\} \sum_{p_j} F_\xi(p_j) \exp\left\{2i n_{\xi j}(\ell+b)\right\}$$

$$+ \sum_{p_j} F_\xi(p_j) \oint \tilde{E}^A_\xi(p_j) \exp(i n_{\xi i}\xi)\, d\xi + \sum_{p_j} F_\xi(p_j) \oint \tilde{E}^A_\xi(p_i) \exp(i n_{\xi j}\xi)\, d\xi$$

$$- 2 R_A \sum_{p_j} F_\xi(p_j) \oint \exp\left\{i(n_{\xi i} + n_{\xi j})\xi\right\} d\xi = 0 , \qquad (31)$$

where $\tilde{E}^A_\xi(p)$ is found from

$$E^A_\xi = \sum_p F_\xi(p)\, \tilde{E}^A_\xi(p) . \qquad (32)$$

In obtaining (31) from (30) we have exploited the stationarity property of Z_A with respect to small perturbations in the current. The integrations in (31) involving simple exponentials may be performed analytically resulting in a set of algebraic equations with the unknowns $F_\xi(p_j)$ and, of course, the antenna impedance Z_A. One of the Fourier components $F_\xi(p_j)$ may be set arbitrarily. The computational procedure consists in solving for the remaining $F_\xi(p_j)$ using an initial guess for Z_A, then using (30) to determine Z_A itself in terms of $F_\xi(p_j)$. The iterations are terminated when Z_A obtained from (30) and (31) acquires the desired accuracy.

IV. THE BOUNDARY VALUE SOLUTION

For the present case of boundaries uniform in the y- and z-directions, the effect of the boundaries may be simulated by the surface current distribution

$$\underline{\underline{J}} = \left[J_y^W \quad J_z^W \quad J_z^F \quad J_y^P \quad J_z^P \right] \tag{33}$$

where the subscripts W, F and P refer to the wall, the Faraday shield and the plasma, respectively. The field components θ_ν^J due to the surface current distribution $\underline{\underline{J}}$

are readily determined using Maxwell's equations and the boundary conditions involving the discontinuity in the tangential magnetic field components at the location of the surface currents. One obtains

$$\Theta_\nu^J = \sum_{k=1}^{5} \sum_m \sum_n J_k \Psi_k N_{k\nu} \exp\left\{i(n_y y + n_z z)\right\}, \quad (34)$$

where

$$\underline{\underline{\Psi}} = \left[\mathcal{E}(x+c) \quad \mathcal{E}(x+c) \quad \mathcal{E}(x-f) \quad \mathcal{E}(x-a) \quad \mathcal{E}(x-a)\right], \quad (35)$$

$$\underline{\underline{N}} =$$

$$\begin{bmatrix} u_{x+c} n_y/2 & \alpha_1 & \alpha_2 & \alpha_5 & 0 & -u_{x+c}/2 \\ u_{x+c} n_z/2 & \alpha_2 & \alpha_3 & \alpha_4 & u_{x+c}/2 & 0 \\ u_{x-f} n_z/2 & \alpha_2 & \alpha_3 & \alpha_4 & u_{x-f}/2 & 0 \\ u_{x-a} n_y/2 & \alpha_1 & \alpha_2 & \alpha_5 & 0 & -u_{x-a}/2 \\ u_{x-a} n_z/2 & \alpha_2 & \alpha_3 & \alpha_4 & u_{x-a}/2 & 0 \end{bmatrix} \quad (36)$$

$$\alpha_1 = -i\,(n_y^2 - 1)\; N_x^{-1}\,/2\;, \tag{37}$$

$$\alpha_2 = -i\;\; n_y\, n_z\;\; N_x^{-1}\,/2\;, \tag{38}$$

$$\alpha_3 = -i\,(n_z^2 - 1)\; N_x^{-1}/2\;, \tag{39}$$

$$\alpha_4 = \;\; i\;\, n_y\; N_x^{-1}\,/2\;, \tag{40}$$

and

$$\alpha_5 = -i\, n_z\; N_x^{-1}\,/2\;. \tag{41}$$

The total electromagnetic field $\underline{\underline{\Theta}}$ due to the antenna and the surface currents must satisfy the boundary conditions

$$E_y(-c) - \zeta_w\, J_y^w \;\; = 0\;, \tag{42}$$

$$E_z(-c) - \zeta_w\, J_z^w \;\; = 0\;, \tag{43}$$

$$E_z(f) - \zeta_F\, J_z^F \;\; = 0\;, \tag{44}$$

$$E_y(a) - \zeta_{fs} H_y(a) - \zeta_{ff} H_z(a) = 0, \tag{45}$$

and

$$E_z(a) - \zeta_{ss} H_y(a) - \zeta_{sf} H_z(a) = 0, \tag{46}$$

where, ζ_W and ζ_F, respectively, are the wall and the Faraday shield surface resistances. Writing

$$\Theta_\nu = \Theta_\nu^A + \Theta_\nu^J , \tag{47}$$

where Θ_ν^J is the electromagnetic field due to the surface currents $\underline{\underline{J}}$, (42) to (46) become

$$E_y^J(-c) - \zeta_w J_y^W = -E_y^A(-c) , \tag{48}$$

$$E_z^J(-c) - \zeta_w J_z^W = -E_z^A(-c) , \tag{49}$$

$$E_z^J(f) - \zeta_F J_z^F = -E_z^A(f) , \tag{50}$$

$$E_y^J(a) - \zeta_{fs} H_y^J(a) - \zeta_{ff} H_z^J(a) = -E_y^A(a) + \zeta_{fs} H_y^A(a) + \zeta_{ff} H_z^A(a) , \tag{51}$$

and

$$E_z^J(a) - \zeta_{ss} H_y^J(a) - \zeta_{sf} H_z^J(a) = -E_z^A(a) + \zeta_{ss} H_y^A(a) + \zeta_{sf} H_z^A(a) . \tag{52}$$

The right hand sides of (48)-(52) involve known quantities, namely, the surface impedance matrix $\underline{\underline{\zeta}}_p$ and the antenna electromagnetic field $\underline{\underline{\Theta}}^A$ already determined in Sec. III. The left hand sides contain, in addition to $\underline{\underline{\zeta}}_p$, $\underline{\underline{\Theta}}^J$ resulting from the surface currents $\underline{\underline{J}}$. Writing $\underline{\underline{\Theta}}^J$ in terms of $\underline{\underline{J}}$ using (34)-(41) reduces (48)-(52) to a set of linear algebraic equations in the five unknown surface currents, with the matrix solution

$$\underline{\underline{J}} = \underline{\underline{\Phi}}\ \underline{\underline{M}}^{-1} \tag{53}$$

where

$$\underline{\underline{\Phi}} =$$

$$\left[-E_y^A(-c) \quad -E_z^A(-c) \quad -E_z^A(f) \quad \left\{-E_y^A(a)+\zeta_{fs}H_y^A(a)+\zeta_{ff}H_z^A(a)\right\} \quad \left\{-E_z^A(a)+\zeta_{ss}H_y^A(a)+\zeta_{sf}H_z^A(a)\right\}\right] \tag{54}$$

and

$$\underline{\underline{M}} =$$

$$\begin{bmatrix}
(\alpha_1 - \varrho_w) & \alpha_2 & \alpha_2 \varepsilon(c+f) & (\alpha_1 + \varrho_{ff}/2)\varepsilon(a+c) & (\alpha_2 + \varrho_{sf}/2)\varepsilon(a+c) \\
\alpha_2 & (\alpha_3 - \varrho_w) & \alpha_3 \varepsilon(c+f) & (\alpha_2 - \varrho_{fs}/2)\varepsilon(a+c) & (\alpha_3 + \varrho_{ss}/2)\varepsilon(a+c) \\
\alpha_2 \varepsilon(c+f) & \alpha_3 \varepsilon(c+f) & (\alpha_3 - \varrho_F) & (\alpha_2 - \varrho_{fs}/2)\varepsilon(a-f) & (\alpha_3 + \varrho_{ss}/2)\varepsilon(a-f) \\
\alpha_1 \varepsilon(a+c) & \alpha_2 \varepsilon(a+c) & \alpha_2 \varepsilon(a-f) & (\alpha_1 - \varrho_{ff}/2) & (\alpha_2 + \varrho_{sf}/2) \\
\alpha_2 \varepsilon(a+c) & \alpha_3 \varepsilon(a+c) & \alpha_3 \varepsilon(a-f) & (\alpha_2 - \varrho_{fs}/2) & (\alpha_3 - \varrho_{ss}/2)
\end{bmatrix}$$

(55)

Thus (53) determines $\underline{\underline{J}}$ which, in turn, using (34) determines $\underline{\underline{\Theta}}^J$, the electromagnetic field component due to the surface currents. Adding to it $\underline{\underline{\Theta}}^A$, the antenna field derived in Sec. III finally gives the total electromagnetic field $\underline{\underline{\Theta}}$ using (47).

Since Φ_ν in (54) may be expressed in the form (32) as

$$\underline{\Phi}_\nu = \sum_p F_\xi(p)\, \underline{\tilde{\Phi}}_\nu(p) , \tag{56}$$

the total tangential (to the antenna surface) electric field is expressible in the form

$$E_\xi = \sum_p F_\xi(p) \left\{ \tilde{E}_\xi^A(p) + \tilde{E}_\xi^J(p) \right\} , \tag{57}$$

where

$$\sum_p F_\xi(p)\, \tilde{E}_\xi^J(p) = E_\xi^J(p) , \tag{58}$$

$E_\xi^J(p)$ being the tangential electric field produced by the surface currents $\underline{J}$. The determination of the self-consistent antenna current, then involves steps identical to those outlined in Sec. III D, with the stipulation that the total tangential electric field E_ξ replaces the antenna electric field E_ξ^A.

V. APPLICATION TO FAST WAVE COUPLING AT THE ION CYCLOTRON RANGE OF FREQUENCIES

As an illustration of the loop antenna theory, we consider coupling to a semi-infinite plasma slab immersed in a uniform magnetic field B_o, with a density profile assumed to vary linearly from $n_e(x=a) = 0$ to $n_e(x=x_p+a) = \tilde{n}_e$, where tilde denotes the absolute maximum value. The plasma surface impedance components $\mathcal{S}_{ff}(m,n)$ and $\mathcal{S}_{ss}(m,n)$ for this case may be analytically determined[17, 18]. More complicated density profiles would require numerical integration of the Maxwell's equations. An elegant analytical approach for the determination of $\mathcal{S}_{ff}$ for arbitrary density profiles using Epstein's[19] method has also been recently developed by Bhatnagar et al.[20]. In this paper, however, we are primarily concerned with the antenna theory and will not further delve into questions connected with the treatment of the plasma impedance matrix; nor indeed enter into the subtleties of ICRF heating schemes.

Using the parameters of Table 1 and the procedure outlined in Secs. III and IV, one obtains the antenna impedance Z_A and the antenna input power, P_A, for unit applied voltage at the antenna terminals as a function of frequency (Fig. 2). Also, ideally

$$P_A = P_P + L_A + L_F + L_W , \qquad (59)$$

where P_P is the Poynting vector into the plasma while L_A, L_F and L_W are the antenna, Faraday shield and the wall losses, respectively. That such a condition is approached to within a few percent is a confirmation of the computational accuracy.

The computations performed on the CRAY 1 computer require approximately three minutes per run for the parameters listed in Table 1. The run time varies linearly with m_{max} and n_{max} and quadratically with p_{max}. For most cases of interest sufficiently removed from the region of resonance, both m_{max} and n_{max} may each be reduced to half the present values without significant loss in the accuracy of the results. In most cases, acceptable convergence was obtained for $p_{max} = 5$.

Although (59) is already an extremely demanding test, further confidence in the computations is gained by the fact that when the wall, the plasma, and the Faraday shield are far removed from the antenna, the input impedance values obtained are within 1% of the short circuited transmission line impedance given by

$$Z_{sc} = i\,(b/w)\,\tan(2\ell) . \qquad (60)$$

These computations also confirm the existing results[13, 21, 22], namely, that the antenna propagation constant is principly determined by the antenna, the wall, and the Faraday shield geometry, and is largely unaffected by the presence of the plasma. It will be subsequently pointed out in Sec. VI how this property may be utilized to introduce the concept of reflectionless coupling.

VI. DISCUSSION

A. The $F_z(n)$ spectrum

In the computations of Sec. V, it was assumed that the current was uniformly distributed over the antenna width 2w, so that $F_z(n)$ in (8) is given by

$$F_z(n) = n_{zo} \sin(n_z w) / (\pi w n_z) . \quad (61)$$

As a result of this assumption the integrand

$$V(z) = \oint E_\xi(\xi)\, d\xi = -\int_{-b}^{b} dx \int_{-l}^{l} dy\, H_z(z), \quad (62)$$

is maximum at z=0 with a mild taper towards the edges. Since $E_\xi(\xi)$ at z=0 was employed in the variational formulation, Z_A obtained from (30) tends to be somewhat large resulting in the discrepancy noted in P_A exceeding the right hand side by approximately 3% in (59). The situation could be remedied by taking a current profile slightly peaked at the edges, so that V(z) is constant over the antenna width. This would also reduce the E_z field over the antenna surface (an important boundary condition, conspicuous by its absence in the variational formulation of Storer[14], which is strictly applicable for thin antennas only). That such an effort is not called for in practice is attested by the fact that the antenna voltage varies by a negligible extent ($\sim$ 3 %) over the antenna width. A more ambitious undertaking would, in addition, require the inclusion of the transverse antenna currents J_z^A which were neglected at the outset.

B. The Faraday shield

The perfect alignment of the Faraday shield along B_o assumed in this analysis precludes E_z and the attendant coupling to the slow (lower-hybrid) or the ion-Bernstein waves. Assuming, however, that a small angle φ exists between the Faraday shield conductors and B_o, would result

in E_z given approximately by

$$E_z \approx E_y \sin\varphi \approx E_y \varphi \,. \tag{63}$$

The energy coupled into the fast and the slow waves, respectively, is given by

$$P_f = \mathrm{Re}\left[(1/2)\, E_y H_z^*\right] = \mathrm{Re}\,(1/2)\,|E_y|^2 / \varepsilon_{ff}^* \,, \tag{64}$$

$$P_s = \mathrm{Re}\left[-(1/2)\, E_z H_y^*\right] = \mathrm{Re}\,(1/2)\,|E_z|^2 / \varepsilon_{ss}^* \,. \tag{65}$$

The relative power input into the two waves is given by,

$$\gamma = P_s / P_f = \varphi^2 \left(\varepsilon_{ss}^R / \varepsilon_{ff}^R\right) \left|\varepsilon_{ff} / \varepsilon_{ss}\right|^2 \,. \tag{66}$$

Inserting the expressions for ε_{ff} and ε_{ss} (for the case $n_y = 0$) from Refs. 18 and 23, respectively, one obtains

$$\gamma = \frac{2^{1/3}}{3^{1/2}} \left(\frac{m_i}{m_e}\right)^{1/3} \left(n_z^2 - 1\right)^{-2/3} \varphi^2 \tag{67}$$

Thus for φ corresponding to 3^o, and $n_z = 3$, approximately 1% of the energy is coupled to the slow wave.

For a relatively clean plasma, as in the case of ASDEX, the slow wave converts to the ion-Bernstein waves and is eventually absorbed by a combination of electron

Landau damping and ion-cyclotron damping in the plasma bulk, and one might consider dispensing with the Faraday screen altogether. Less benign effects might, however, accompany if the impurity harmonics dominate, leading to surface heating of both the electron and the impurity ion species[24,25].

In case the plasma density at the antenna surface already exceeds the requirement for the lower-hybrid resonance, the ion-Bernstein waves will be launched directly[25, 26] with ε_{ss} (n_y=0) given in Ref. 18. For this case, $\gamma < O(\varepsilon^2)$ for the parameters of Table 1.

The above estimates are provided in order to illustrate an important concept. A more precise answer must await an exact boundary value solution which at the outset allows an inclination between the Faraday shield and B_o and, of course, the inclusion of $n_y \neq 0$ terms.

Nor does the story with the slow wave coupling end here. The part of the fast wave not absorbed in a single pass through the plasma would be subject to significant scattering from wall imperfections of size comparable to the wavelengths Λ_{yo}/m and Λ_{zo}/n. The ensuing change in polarization will continually divert the fast wave energy into the slow waves which may assume an important role in the energy absorption process.

Another key role played by the Faraday screen consists of reactive loading of the antenna considered as a transmission line[13, 21, 22]. How this property may be put to advantage is described in the following section (VI C).

C. Impedance matching

The impedance values obtained for the ICRF coupling (Sec. V) are well suited for experimental purposes. Yet in the face of variable plasma conditions, one would require complex matching networks to create optimal coupling. One possible way out is an antenna long enough to preclude a reflected wave. In addition, the characteristic impedance Z_o, principally determined (see Sec. V) by the antenna width and separation from the Faraday screen[13,21,22], can be made equal to the generator impedance, thereby creating an improved impedance match - a considerable boon for the experimentalist.

A reactively loaded spiral antenna (Fig. 3) would give rise to a transmission line with a reasonably constant characteristic impedance. This geometry will create efficient coupling conditions at low frequencies corresponding to Alfvén wave hating of ICRF heating at low harmonics, tapering off in efficacy as the frequency is raised.

At higher frequencies where the antenna length 2ℓ is comparable to the rf half wavelength, one may employ a meander antenna (or a number of similar alternatives), shown in Fig. 4. For such an antenna the coupling efficiency would diminish as the frequency is lowered; yet a considerable advantage in the form of a matched-load (dictated by the fairly constant impedance transmission line formed between the antenna and the Faraday screen) termination may be available. Similar ideas of reflectionless coupling have been previously advanced by Lisitano[27].

APPENDIX A

Plasma surface impedance matrix

Let α and β be the amplitudes of a set of two waves with non-identical polarizations at the arbitrarily prescribed surface $x = x_{\alpha\beta}$ in the geometry consisting solely of the semi-infinite plasma slab with boundary at x=a. Then α and β together with the wave polarizations uniquely determine the electromagnetic field $\theta_\nu = \theta^\alpha_\nu + \theta^\beta_\nu$. Specifically at the vacuum plasma boundary (x=a)

$$E_y = \alpha E_y^\alpha + \beta E_y^\beta , \qquad \text{(A 1)}$$

$$E_z = \alpha E_z^\alpha + \beta E_z^\beta , \qquad \text{(A 2)}$$

$$H_y = \alpha H_y^\alpha + \beta H_y^\beta , \qquad \text{(A 3)}$$

and

$$H_z = \alpha H_z^\alpha + \beta H_z^\beta . \qquad \text{(A 4)}$$

Eliminating α and β, one may rewrite

$$E_y = \varrho_{fs} H_y + \varrho_{ff} H_z , \qquad \text{(A 5)}$$

and

$$E_z = \varrho_{ss} H_y + \varrho_{sf} H_z , \qquad \text{(A 6)}$$

where

$$\varrho_{ff} = (E_y^{\beta} H_y^{\alpha} - E_y^{\alpha} H_y^{\beta}) \Delta^{-1} , \qquad \text{(A 7)}$$

$$\varrho_{fs} = (E_y^{\alpha} H_z^{\beta} - E_y^{\beta} H_z^{\alpha}) \Delta^{-1} , \qquad \text{(A 8)}$$

$$\varrho_{ss} = (E_z^{\alpha} H_z^{\beta} - E_z^{\beta} H_z^{\alpha}) \Delta^{-1} , \qquad \text{(A 9)}$$

$$\varrho_{sf} = (E_z^{\beta} H_y^{\alpha} - E_z^{\alpha} H_y^{\beta}) \Delta^{-1} , \qquad \text{(A 10)}$$

and

$$\Delta = (H_y^{\alpha} H_z^{\beta} - H_y^{\beta} H_z^{\alpha}) . \qquad \text{(A 11)}$$

For the case of ICRF heating, if we choose the polarizations for the α and β to be along y and z axes, respectively, the two waves are effectively decoupled. Consequently, E_y^{β}, E_z^{α}, H_y^{α} and H_z^{β} vanish and one obtains

from (A7)-(A11), the well-known results

$$\zeta_{ff} = E_y^{\alpha} / H_z^{\alpha} , \qquad \text{(A 12)}$$

$$\zeta_{fs} = 0 , \qquad \text{(A 13)}$$

$$\zeta_{ss} = - E_z^{\beta} / H_y^{\beta} , \qquad \text{(A 14)}$$

and

$$\zeta_{sf} = 0 . \qquad \text{(A 15)}$$

Apart from nomenclature, the development of $\underline{\underline{\zeta}}_P$ parallels Brambilla's[28] treatment of the plasma surface impedance matrix for the case of lower-hybrid wave coupling.

APPENDIX B

A. Fields due to an elementary excitation

Fields for the spatially repeated (at intervals Λ_{yo}) sheet currents $\hat{x} \exp [i(n_x x + n_y y + n_z z)]$ are given by ($\hat{x}$ is unit vector in the x-direction)

$$E_x = i n_y^{-1} (1 - n_x^2) \mathcal{C} D^{-1} , \qquad \text{(B 1)}$$

$$E_y = n_x \mathcal{S} D^{-1} , \qquad \text{(B 2)}$$

$$E_z = -i n_x n_z \mathcal{C} D^{-1} , \qquad \text{(B 3)}$$

$$H_x = 0 , \qquad \text{(B 4)}$$

$$H_y = i n_y^{-1} n_z \mathcal{C} D^{-1} , \qquad \text{(B 5)}$$

and

$$H_z = \mathcal{S} D^{-1} , \qquad \text{(B 6)}$$

where

$$\mathcal{C} = \cos \left[n_y \{ (y - \ell) - u_{y-\ell} \Lambda_{yo} / 2 \} \right] , \qquad \text{(B 7)}$$

$$S = \sin\left[n_y\{(y-\ell) - u_{y-\ell}\,\Lambda_{yo}/2\}\right] , \qquad \text{(B 8)}$$

and

$$D = 2\sin(n_y\,\Lambda_{yo}/2) . \qquad \text{(B 9)}$$

B. The Green's functions

The Green's functions for the impulse excitation $\delta(x)$ may now be obtained by integrating (B1)-(B6), one at a time, over the Fourier spectrum (14). The integrand consists of residues corresponding to the singularities of D in (B9) which possesses simple poles at

$$n_y\,\Lambda_{yo} = 2m\pi . \qquad \text{(B 10)}$$

The path of integration extends over the real n_x axis from $-\infty$ to $+\infty$ and closes back over a semicircle of Radius $R\to\infty$ in the upper or the lower half plane, respectively, for $x \gtrless 0$. The Green's functions obtained in this manner are given by

$$GE_x = -i \sum_m F\,(1+N_x^2)\,N_x^{-1} , \qquad \text{(B 11)}$$

$$GE_y = -\sum_m F\,u_x\,n_y , \qquad \text{(B 12)}$$

$$G E_z = - \sum_m F u_x n_z \ , \qquad \text{(B 13)}$$

$$G H_x = 0 \ , \qquad \text{(B 14)}$$

$$G H_y = - i \sum_m F n_z N_x^{-1} \ , \qquad \text{(B 15)}$$

and

$$G H_z = i \sum_m F n_y N_x^{-1} \ , \qquad \text{(B 16)}$$

where

$$F = - (n_{y_0} / 4\pi) \, \varepsilon(x) \exp(-i n_y \ell) \exp\{i (n_y y + n_z z)\} . \qquad \text{(B 17)}$$

APPENDIX C

A. The antenna field component E_z

$$E_z^{AF} = i\,(n_{y_o}/2\pi) \sum_m \sum_n \sum_p F(n)\,F(p)\,\varepsilon(x-b)$$

$$\cdot\,(n_y n_z / N_x)(n_y + n_\zeta)^{-1} \exp\{i n_\zeta (\ell+b)\} \sin\{(n_y+n_\zeta)\ell\} \qquad (C\ 1)$$

$$E_z^{A\beta} = -i\,(n_{y_o}/2\pi) \sum_m \sum_n \sum_p F(n)\,F(p)\,\varepsilon(x+b)$$

$$\cdot\,(n_y n_z / N_x)(n_y - n_\zeta)^{-1} \exp\{-i n_\zeta (\ell+b)\} \sin\{(n_y-n_\zeta)\ell\} \qquad (C\ 2)$$

$$E_z^{A S_b} = -i\,(n_{y_o}/2\pi) \sum_m \sum_n \sum_p F(n)\,F(p)\,\varepsilon(x-b)$$

$$\cdot\; N_x n_z (N_x^2 + n_\zeta^2)^{-1} \exp\{i n_\zeta (\ell+b)\}$$

$$\cdot\left[\sin\{(n_y+n_\zeta)\ell\} + u_{x-b}\,(n_\zeta/N_x)\cos\{(n_y+n_\zeta)\ell\}\right] \qquad (C\ 3)$$

$$E_z^{AS_{-b}} = i(n_{y_0}/2\pi) \sum_m \sum_n \sum_p F(n) F(p) \varepsilon(x+b)$$

$$\cdot N_x n_z (N_x^2 + n_3^2)^{-1} \exp\{-i n_3 (\ell+b)\}$$

$$\cdot \left[\sin\{(n_y - n_3)\ell\} + u_{x+b} (n_3/N_x) \cos\{(n_y - n_3)\ell\}\right] ,$$

(C 4)

$$E_z^{AS_0} = i(n_{y_0}/2\pi) \sum_m \sum_n \sum_p F(n) F(p) \varepsilon(x)$$

$$\cdot u_x n_z (\nu_x - i n_3)^{-1} \sin\{2 n_3 (\ell+b)\} ,$$

(C 5)

$$E_z^{AS_T} = -i(n_{y_0}/2\pi) \sum_m \sum_n \sum_p F(n) F(p) \cos\left[n_3\{x - u_x(\ell+b)\} - n_y \ell\right]$$

$$\cdot 2 \square(-b, b) n_z n_3 (N_x^2 + n_3^2)^{-1} \exp\{i n_3 u_x (\ell+b)\} .$$

(C 6)

B. The field components E_x^A, H_x^A, H_y^A and H_z^A

Knowing E_y^A from (16-21) and E_z^A from (C1-C6) one obtains E_x^A from the divergence equation

$$n_x E_x^A + n_y E_y^A + n_z E_z^A = 0 \qquad \text{(C 7)}$$

The magnetic field components are then obtained using the Maxwell's equation

$$\underline{\nabla} \times \underline{E}^A = i \underline{H}^A \qquad \text{(C 8)}$$

In our original derivation of the antenna field in Sec. III, however, all the field components were directly derived from the antenna current distribution. Equations (C7) and (C8) were then employed as a check on the correctness of the algebraic expressions.

Table 1

a	plasma position	10.6 cm
2b	antenna breadth	6.9 cm
2l	antenna height	49.0 cm
2w	antenna width	18.0 cm
f	Faraday shield position	5.5 cm
c-b	wall separation from antenna back	0
x_p	plasma profile width	20.0 cm
$\tilde{n}_e$	maximum plasma density	5×10^{13} cm^{-3}
B_o	magnetic field strength	2.23 T
A	Atomic mass (Hydrogen)	1
λ_o	free space wavelength	429 cm
λ_{yo}	fundamental y-wavelength	251 cm
λ_{zo}	fundamental z-wavelength	258 cm
m_{max}	maximum y-harmonic	37
n_{max}	maximum z-harmonic	37
p_{max}	maximum p-harmonic	5
ρ_A	antenna specific resistance	1.5×10^{-6} Ω-cm
ρ_F	Faraday shield specific resistance	3×10^{-6} Ω-cm
ρ_W	wall specific resistance	90×10^{-6} Ω-cm

FIGURE AND TABLE CAPTIONS

Fig. 1 Geometry of the single loop (a) and of the system (b) comprising of the repeated loops (both along y and z directions at intervals Λ_{yo} and Λ_{zo}, respectively), the plasma, the wall, and the Faraday shield.

Fig. 2 Antenna impedance and input power (for unit applied voltage) as a function of the rf frequency for the parameters of Table 1.

Fig. 3 The spiral antenna.

Fig. 4 The meander antenna.

Table 1 Parameters for the sample ICRF coupling calculations of Sec. V.

REFERENCES AND FOOTNOTES

1 R.R. Weynants, A.M. Messiaen, C. Leblud, and P.E. Vandenplas, "Heating in Toroidal Plasmas", Proceedings of the 2nd Joint Grenoble-Varenna International Symposium (Commission of the European Communities, Brussels), Como, p. 487 (1980)

2 A. Bers, J. Jacquinot, G. Lister, Ref. 1, p. 569

3 J. Adam, J. Jacquinot, Y. Lapierre, and D. Marty, Proceedings of the 4th Topical Conference on Radio-Frequency Plasma Heating (University of Austin, Texas), Paper A1 (1981)

4 A. Bers, L.P. Harten, and A. Ram, Ref. 3, Paper A 16

5 A.M. Messiaen, R.R. Weynants, L. Bral, and R. Koch, Ref. 3, Paper A 23

6 S. Puri, "Heating in Toroidal Plasmas", Proceedings of the 3rd Joint Grenoble-Varenna International Symposium (Commission of the European Communities, Brussels), Grenoble, p. 191 (1982)

7 PLT Team (paper presented by J. Hosea), Ref. 6, p. 213

8 Equipe TFR (paper presented by J. Jacquinot), Ref. 6, p. 225

9 A.M. Messiaen, R. Koch, V.P. Bhatnagar, M.P. Evrard, M. Luwel, P.E. Vandenplas, and R.R. Weynants, Ref. 6, p. 243

10 J. Jacquinot, K. Theilhaber, G. Lister and M. Brambilla, Ref. 6, p. 375

11 A. Ram and A. Bers, Ref. 6, p. 395

12 V.P. Bhatnagar, R. Koch, A. Messiaen, R.R. Weynants, Nuclear Fusion 22, 280 (1982)

13 K. Theilhaber and J. Jacquinot, Report EUR-CEA-FC-1166, Centre d'Etudes Nucléaires, Fontenay-aux-Roses (1982)

14 J.E. Storer, Doctoral Dissertation, Harvard University, Cambridge, MA (1951), Chapter II (published in Ref. 15)

15 R.W.P. King, The Theory of Linear Antennas, Harvard University Press, Cambridge, MA (1956)

16 Except for the case of the principal field component H_z^A.

17 S. Puri, Ref. 6, p. 391 (1982)

18 S. Puri, Phys. Fluids 26, 164 (1983)

19 P.S. Epstein, Proc.Nat.Acad.Sci., Washington, 16, 627 (1930)

20 R.P. Bhatnagar, V.P. Bhatnagar, R. Koch and R.R.Weynants, Plasma Physics 25, 755 (1983)

21 V.P. Bhatnagar, R. Koch, A.M. Messiaen, and R.R.Weynants, Nuclear Fusion 22, 279 (1982)

22 M. Söll (private communication)

23 V.E. Golant, Sov.Phys.-Techn. Phys. 16, 1980 (1972)

24 S. Puri, Proceedings of the Third Topical Conference on Radio-Frequency Heating (California Institute of Technology, Pasadena, 1978)

25 S. Puri, Phys. Fluids 22, 1716 (1979)

26 M. Ono, Princeton University Report No. PPPL-1593 (1979)

27 G. Lisitano, "A method of Radio-Frequency Conditioning of Fusion Plasmas", Report IPP III/87, Max-Planck-Institut für Plasmaphysik, D-8046 Garching (1983)

28 M. Brambilla, Nuclear Fusion 19, 1343 (1979)

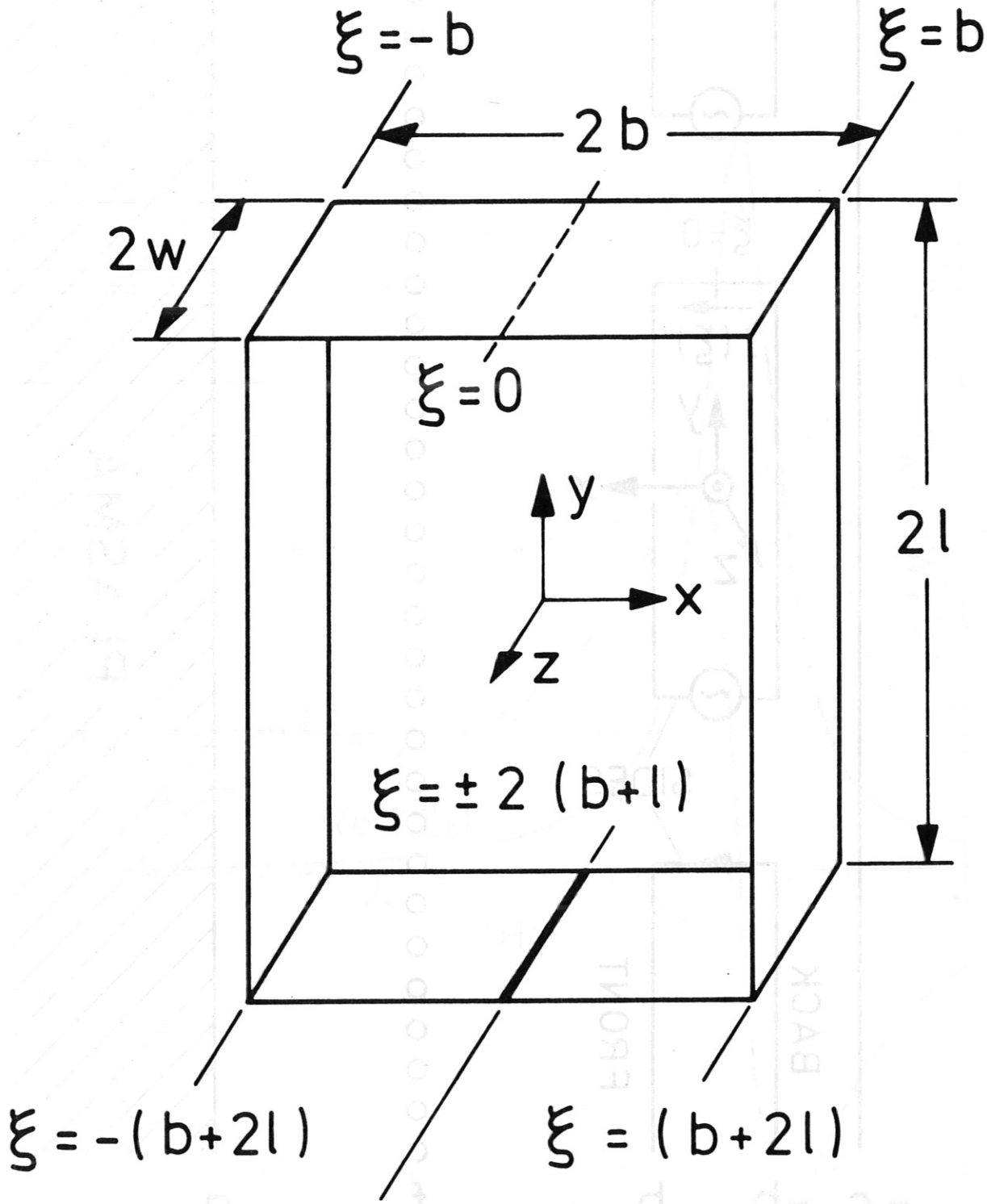
ξ=-b
ξ=b
2b
2w
ξ=0
y
x
z
2l
ξ=±2(b+l)
ξ=-(b+2l)
ξ=(b+2l)
SLICE GENERATOR

ξ=0
I(ξ)
y
x
z
SIDES
BACK
FRONT
-c
-b
b
f
a
PLASMA

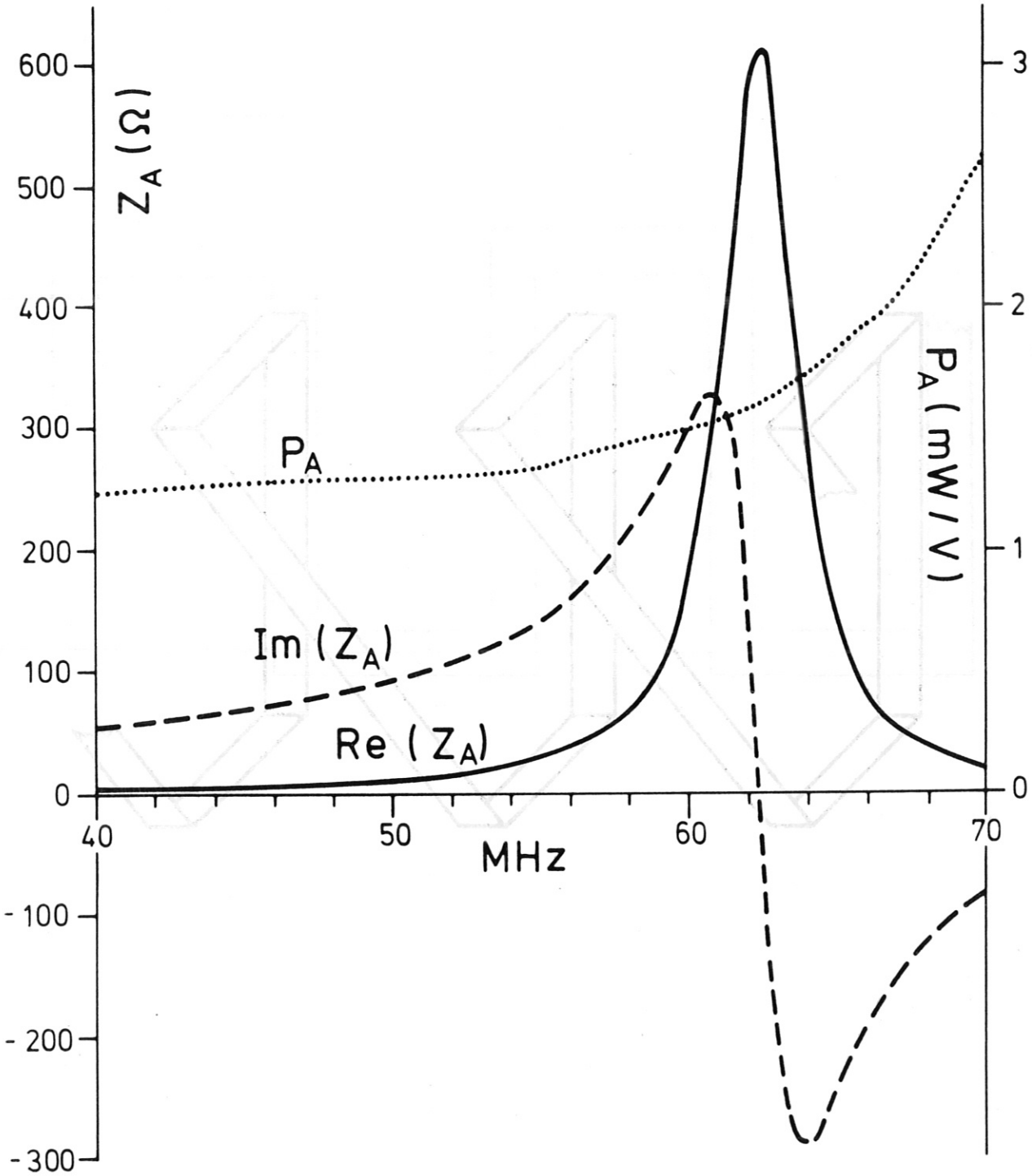
600
500
400
300
200
100
0
- 100
- 200
- 300
Z_A (Ω)
3
2
1
0
P_A (mW / V)
P_A
Im (Z_A)
Re (Z_A)
40
50
60
70
MHz